minerals

MDPI

Article

Performance Evaluation of Fe-Al Bimetallic Particles for the Removal of Potentially Toxic Elements from Combined Acid Mine Drainage-Effluents from Refractory Gold Ore Processing

Elham Aghaei [1], Zexiang Wang [1], Bogale Tadesse [1], Carlito Baltazar Tabelin [2], Zakaria Quadir [3] and Richard Diaz Alorro [1,*]

[1] Western Australian School of Mines: Minerals, Energy and Chemical Engineering, Faculty of Science and Engineering, Curtin University, Kalgoorlie, WA 6403, Australia; elham.aghaei@postgrad.curtin.edu.au (E.A.); zexiang.wang@postgrad.curtin.edu.au (Z.W.); bogale.tadesse@curtin.edu.au (B.T.)

[2] School of Minerals and Energy Resources Engineering, Faculty of Engineering, University of New South Wales, Sydney, NSW 2052, Australia; c.tabelin@unsw.edu.au

[3] John de Laeter Centre and School of Civil and Mechanical Engineering, Faculty of Science and Engineering, Curtin University, Bentley, WA 6845, Australia; zakaria.quadir@curtin.edu.au

* Correspondence: Richard.Alorro@curtin.edu.au; Tel.: +61-890886187

Abstract: Acid mine drainage (AMD) is a serious environmental issue associated with mining due to its acidic pH and potentially toxic elements (PTE) content. This study investigated the performance of the Fe-Al bimetallic particles for the treatment of combined AMD-gold processing effluents. Batch experiments were conducted in order to eliminate potentially toxic elements (including Hg, As, Cu, Pb, Ni, Zn, and Mn) from a simulated waste solution at various bimetal dosages (5, 10, and 20 g/L) and time intervals (0 to 90 min). The findings show that metal ions with greater electrode potentials than Fe and Al have higher affinities for electrons released from the bimetal. Therefore, a high removal (>95%) was obtained for Hg, As, Cu, and Pb using 20 g/L bimetal in 90 min. Higher uptakes of Hg, As, Cu, and Pb than Ni, Zn, and Mn also suggest that electrochemical reduction and adsorption by Fe-Al (oxy) hydroxides as the primary and secondary removal mechanisms, respectively. The total Al^{3+} dissolution in the experiments with a higher bimetal content (10 and 20 g/L) were insignificant, while a high release of Fe ions was recorded for various bimetal dosages. Although the secondary Fe pollution can be considered as a drawback of using the Fe-Al bimetal, this issue can be tackled by a simple neutralization and Fe precipitation process. A rapid increase in the solution pH (initial pH 2 to >5 in 90 min) was also observed, which means that bimetallic particles can act as a neutralizing agent in AMD treatment system and promote the precipitation of the dissolved metals. The presence of chloride ions in the system may cause akaganeite formation, which has shown a high removal capacity for PTE. Moreover, nitrate ions may affect the process by competing for the released electrons from the bimetal owing to their higher electrode potential than the metals. Finally, the Fe-Al bimetallic material showed promising results for AMD remediation by electrochemical reduction of PTE content, as well as acid-neutralization/metal precipitation.

Keywords: acid mine drainage; gold processing effluents; Fe-Al bimetallic particles; electrochemical reduction

Citation: Aghaei, E.; Wang, Z.; Tadesse, B.; Tabelin, C.B.; Quadir, Z.; Alorro, R.D. Performance Evaluation of Fe-Al Bimetallic Particles for the Removal of Potentially Toxic Elements from Combined Acid Mine Drainage-Effluents from Refractory Gold Ore Processing. *Minerals* **2021**, *11*, 590. https://doi.org/10.3390/min11060590

Academic Editor: Juan Antelo

Received: 19 April 2021
Accepted: 27 May 2021
Published: 31 May 2021

1. Introduction

Acid mine drainage (AMD) refers to acidic runoff rich in high concentrations of metal ions, such as iron (Fe), manganese (Mn), zinc (Zn), copper (Cu), lead (Pb), nickel (Ni), arsenic (As), cadmium (Cd), aluminum (Al), and mercury (Hg) [1–3]. AMD is associated with mining and mineral processing activities and comes from the natural oxidation of sulfide-bearing minerals (such as pyrite) exposed to water, oxygen, and microbes [4,5]. AMD is considered one of the most prevalent causes of environmental pollution which stems from its high acidity (pH < 3) and toxic metal content [6]. Tailings waste from

processing of refractory gold ores is one of the major areas of concern as it contains sulfide species and is very likely to produce AMD over time, especially in dry climates and high evaporation rates [7]. Therefore, parts of tailings with sulfide minerals content exposed to air will start to oxidize during summer to form AMD.

To tackle the issue of AMD, many attempts have been made to limit the generation and release of AMD by protecting sulfide minerals from air, water, and bacteria and minimizing their interactions [5,8–13]. However, due to practical constraints involved in the prevention strategy [14], the next available option is AMD treatment by either active or passive methods [2]. The most common active methods include neutralization using caustic soda (sodium hydroxide), calcium hydroxide ($Ca(OH)_2$) or limestone ($CaCO_3$), as well as adsorption, ion exchange, and crystallization [6,15]. However, the interest in improving the efficiency of AMD remediation techniques motivated researchers to develop passive methods, which involves biological and chemical treatment of AMD using wetlands [16], permeable reactive barriers [17,18], compost reactors, and bioreactors, and cost-effective materials such as recycled concrete aggregates [14], sulfur-reducing bacteria (SRB) [19], and fly ash [20]. Studies with AMD have focused on neutralizing the acidity and heavy metal removal. However, in the case of combined AMD-waste effluents resulting from refractory gold processing with Cl^- and NO_3 content, it has not been considered anywhere before.

When exploring the most appropriate treatment techniques, it is crucial to consider the use of non-toxic, cost-effective, and high-performance materials with the lowermost potential of hazardous wastes/bi-products generation. Accordingly, zero-valent iron (ZVI) has been considered a promising element for removal of heavy metals and PTE from the aquatic environment [21] and the most common reactive material used in permeable reactive barriers (PRBs) for remediating AMD and contaminated groundwater [22]. Depending on the environmental conditions (pH, redox, and oxic-anoxic conditions), type and concentration of dissolved constituents; ZVI can remove heavy metals and PTE from solutions effectively through adsorption, surface complexation, reductive precipitation, and co-precipitation [3,22]. However, one major drawback with this kind of application is the decreasing reactivity and performance of ZVI in the long-term due to iron corrosion and surface passivation by an iron oxy-hydroxide film [21,22]. Recently, iron-based bimetallic materials have been developed aimed at improving the reactivity and efficiency of ZVI in removing PTE. In this regard, due to the synergistic effect of Fe and Al, the Fe-Al bimetal has shown remarkably improved reductive ability for the contaminants [23]. The potential difference between Fe and Al ($E^0(Al^{3+}/Al^0) = -1.667$ V and $E^0(Fe^{2+}/Fe^0) = -0.44$ V) promotes better electron transfer within the bimetallic system and slows the passivation of the Fe surface, resulting in a higher reducing capacity for target contaminants [24].

A number of studies have examined the performance of Fe-Al bimetallic particles for their ability to remove heavy metals, including Cr(VI) [25], As(III) [26], U(VI) [27] from waste solutions. Their findings demonstrated the high capacity, selectivity, and rapid removal rate of target metal ions by the bimetal, predominantly through electrochemical reduction. Moreover, in a study by Han et al. (2016) [28], a higher removal efficiency for aqueous heavy metal ions (Cr(VI), Cd(II), Ni(II), Cu(II), and Zn(II)) was achieved by acid-washed ZVAl/ZVI mixture in PRBs compared to acid-washed ZVAl or ZVI alone. One significant finding to emerge from this previous study was that the Fe-Al bimetal formation during the reaction has been identified as a major contributing factor to the high removal efficiency. Despite previous studies describing Fe-Al bimetal as a potential technique in wastewater remediation, the direct application of this bimetal in AMD treatment has not been reported to date. According to standard electrode potential of Fe, Al and metals found in AMD such as Pb, Cu, Hg, and Zn, it is clear that the Fe-Al bimetallic material is an effective medium for treating AMD. Compared to common passive treatment methods, which suffer from long processing time [29], Fe-Al bimetallic particles are fast and effective for metal removal. Moreover, both Al and Fe are among the most abundant elements on the earth, and the amount of required bimetal for AMD remediation, and waste generated, is very small. Therefore, this paper evaluates the performance of the Fe-Al bimetal for acid-

neutralization and removal of potentially toxic elements from simulated AMD combined with gold processing effluents by considering the influencing parameters including bimetal dosage and reaction time.

2. Materials and Methods

2.1. Preparation of Combined AMD-Waste Effluent from Refractory Gold Processing

The combined AMD prepared in this study represents the combination of AMD and effluents resulting from the processing of refractory gold ores containing sulfide minerals in the Goldfields region of Western Australia. Parts of tailings from these processing plants, exposed to atmospheric conditions, are very liable to generate AMD over time. The gold processing tailings dam contains Cl^-, and $NO_3{}^-$ ions because of using hydrochloric acid (HCl) or nitric acid (HNO_3) in the acid washing stage [30] and lead nitrate in cyanidation [31,32]. Moreover, scaling up the mining and processing operations has risen the demand for groundwater sources. The available source of process water in Australia, especially in arid regions, is hypersaline groundwater with high Cl^- content [33,34]. With regard to what mentioned above, the combined AMD solution was prepared using 1000 mg/L single-element standard solutions of Mn, Pb, As, Ni, Cu, Zn, and Hg in 2% nitric acid (Sigma-Aldrich), as well as calcium chloride ($CaCl_2$), sodium chloride (NaCl) and ferrous sulfate ($FeSO_4$). The initial pH of the prepared solution was adjusted to 2 using sodium hydroxide (NaOH). The synthetic AMD was with initial metal concentrations shown in Table 1.

Table 1. Initial solute concentrations (mg/L) in the synthetic AMD-gold processing effluents.

Hg	Al	Ca	Mn	Na	Fe	As	Pb	$SO_4{}^{2-}$	Ni	Cu	Zn
32.5	1.4	273.6	36.3	10,896.0	388.4	9.3	91.4	652.0	18.2	53.4	31.9

2.2. Synthesis of Fe-Al Bimetallic Particles

All the reagents used in this study were of analytical grade. The Fe-Al bimetallic particles were synthesized using ZVAl powder (D90 = 86.5 µm) obtained from Barnes (NSW, Australia), and ferric chloride ($FeCl_3{\cdot}6H_2O$, >99% purity) purchased from Chemsupply (SA, Australia). Fe-Al bimetals were prepared by optimizing the procedure used by Chen et al. (2008) [24] and Fu et al. (2015) [25], which are based on the electrochemical reduction and deposition of iron on the ZVAl surface. The first step was to remove the unreactive layer of aluminum oxide from ZVAl using acid washing, in which 20 mL of 1 M hydrochloric acid (HCl) was added to flasks containing 3 gr ZVAl in a shaking incubator and agitated for 15 min at 40 °C and 110 rpm. This treatment was followed by the cementation step by adding 30 mL Fe^{3+} solutions with a certain concentration (to give 0.5 g Fe to 1 gr Al) to the flasks and agitating for 30 min. Then, the Fe/Al particles were recovered and rinsed with deionized water, and dried in a vacuum desiccator. The residual Fe and Al concentrations in the solution was measured (data not shown) to calculate the total Fe and Al content of recovered bimetallic particles in each preparation batch as 1 g Fe/2.1 g Al (±0.05 for 3 samples) (Equations (1) and (2)).

$$Fe_T = Fe_0 - Fe_r \quad (1)$$

$$Al_T = Al_0 - Al_r \quad (2)$$

where

Fe_T and Al_T are the total Fe and Al content of the bimetal,
Fe_0 and Al_0 are applied Fe and Al content, and
Fe_r and Al_r are residual Fe and Al ions concentrations.

2.3. Analytical Techniques

The concentration of dissolved ions were analyzed using inductively coupled plasma optical emission spectroscopy (ICP-OES) and mass spectroscopy (ICP-MS). X-ray powder diffraction (XRD) of bimetallic particles was performed using an Olympus diffractometer (Olympus Scientific Solutions Americas, USA) with Co-Kα radiation source in the range between 5 and 55° (2θ). To characterize the size distribution of ZVAl powder and bimetallic particles, Mastersizer Malvern 3000 was used (Malvern Instruments Ltd., Malvern, UK). The structure and elemental mapping of the bimetal were determined using a Tescan Clara field emission scanning electron microscope (SEM) equipped with an energy dispersive spectrometer (EDS) manufactured by the Oxford Instrument, Oxfordshire, UK).

2.4. Experimental Procedure

To investigate the combined AMD treatment using Fe-Al bimetallic particles, batch experiments were conducted in an incubator shaker at 110 rpm and 25 °C with varying time intervals from 10 to 90 min. In each batch, a specific amount of Fe-Al bimetals (5, 10, and 20 g/L) was added to Erlenmeyer flasks containing 25 mL of the prepared waste solution. No acid or alkali was subsequently added to control the pH during the reaction. All experiments were conducted in duplicate, and average values were presented. After a specified time, the solution content of each flask was recovered by filtration and analyzed for heavy metal concentrations. The percentage of heavy metal removal (% R) was calculated using Equation (3):

$$\%R = \frac{C_0 - C}{C_0} \times 100 \quad (3)$$

where C_0: Initial heavy metal ion concentration, mg/L, and C: Residual heavy metal ion concentration, mg/L.

Stabilities of pollutants were modelled by the Geochemist's Workbench® [35] with the THERMODDEM database [36] based on measured solute activities in the experiments.

3. Results and Discussion

3.1. Characterization of the Fe-Al Bimetallic Particles

The particle size distribution of the ZVAl and the synthesized Fe-Al bimetallic material is illustrated in Figure 1. The graph shows that there was an increase in the particle size of the Fe-Al bimetal compared to ZVAl. Ninety percent of the ZVAl distribution has a smaller particle size of 86.5 µm (D_{90}) while this value increased to 134 µm after acid washing and loading with Fe. Moreover, the diffraction peaks at 45.0° for both Al and Fe and 52.5° for Fe in the XRD pattern (Figure 2) confirmed the presence of both Al and Fe in the bimetal structure.

In addition, the core-shell structure of the bimetal has been detected in the SEM mapping (Figure 3). From the EDS spectra shown in Figure 3, it can be seen that Al is mostly found in the core while Fe is the dominant element on the surface of Al.

3.2. pH Monitoring

The pH plays a vital role in the AMD treatment as increasing in pH can lead to the dissolved metal and hydroxides precipitation [37]. Figure 4 shows the experimental data for the solution pH at a different time and bimetal dosage. As illustrated in the graph, a clear trend of increasing pH with time from 0 to 30 min for all bimetal dosage at initial pH 2 was observed. However, from 30 to 90 min, a slight change in the pH was recorded. In addition, for the combined AMD treated with the greater bimetal dosages, the higher pH values were obtained. The pH of the solution containing 20 g/L of bimetal reached more than 5.5 after 30 min, although it exhibited a slight decrease from 60 to 90 min. The Eh of the solutions was 0.5 V at initial pH of 2 just before adding the bimetal and decreased to minimum value of around 0.21 V in 90 min for all bimetal dosages.

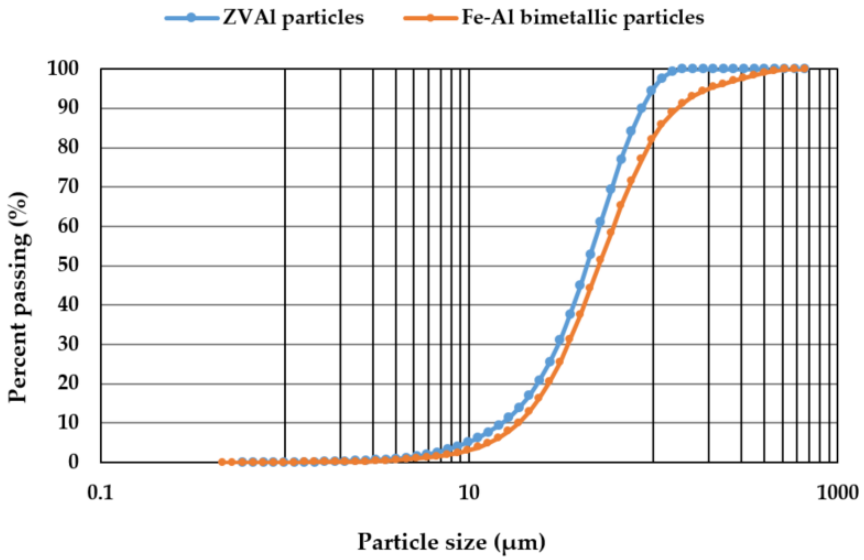

Figure 1. Cumulative particle size distribution of ZVAl and Fe-Al bimetallic material.

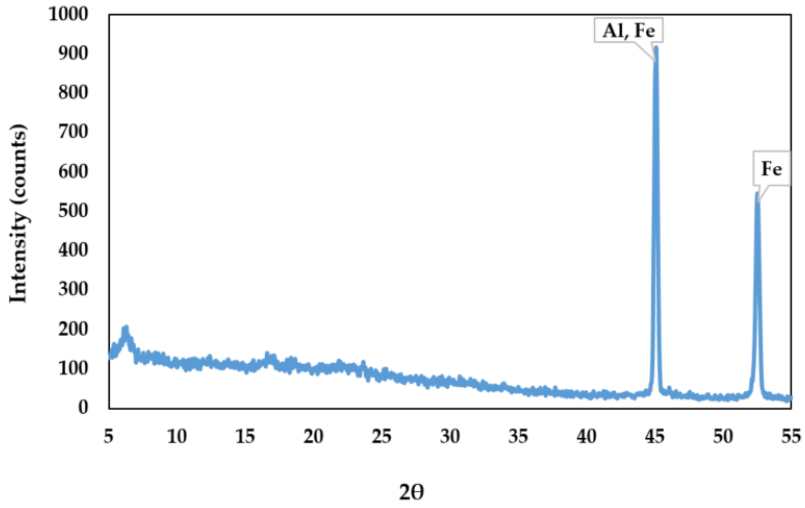

Figure 2. XRD pattern for the synthesized Fe-Al bimetal.

In the acidic aqueous system containing Fe-Al bimetallic particles and dissolved oxygen, the oxidation of ZVAl to Al^{3+} ($E^0(Al^{3+}/Al^0) = -1.667$ V) and ZVI to Fe^{2+} ($E^0(Fe^{2+}/Fe^0) = -0.44$ V) (Equations (4) and (5)) was accompanied by oxygen reduction in the presence of protons (H^+) and the generation of hydrogen peroxide (H_2O_2) ($E^0(O_2/H_2O_2)$= +0.695 V) [38] (Equations (6) and (7)) [38,39]. Hydrogen peroxide subsequently accelerated the ZVAl corrosion to Al^{3+} (Equation (8)) [40,41] and triggered a Fenton reaction, where Fe^{2+} and H_2O_2 reacted to form Fe^{3+}, hydroxyl radicals ($OH^{\cdot}$), and hydroxyl ions (OH^-) (Equation (9)) [38]. In addition, more OH^- released into the solution, where H_2O in the solution picked up electrons. The evolution of H_2 gas resulted from H_2O/H^+ reduction in the solution was also evident in the experiments (Equations (10) and (11)). To sum up, increasing the solution pH is obviously related to the release of OH^- ions into the solution via several reactions in the solution, as discussed above.

$$Al^0 \rightarrow Al^{3+} + 3e^- \quad (4)$$

$$Fe^0 \rightarrow Fe^{2+} + 2e^- \quad (5)$$

$$O_2 + H^+ + e^- \rightarrow HO_2^{\cdot} \quad (6)$$

$$2HO_2 \rightarrow H_2O_2 + O_2 \quad (7)$$

$$Al^0 + 3H_2O_2 \rightarrow Al^{3+} + 3OH^{\cdot} + OH^- \quad (8)$$

$$Fe^{2+} + H_2O_2 \rightarrow Fe^{3+} + OH^{\cdot} + OH^- \quad (9)$$

$$2H_2O + 2e^- \rightarrow H_2 + 2OH^- \quad (10)$$

$$2H^+ + 2e^- \rightarrow H_2 \quad (11)$$

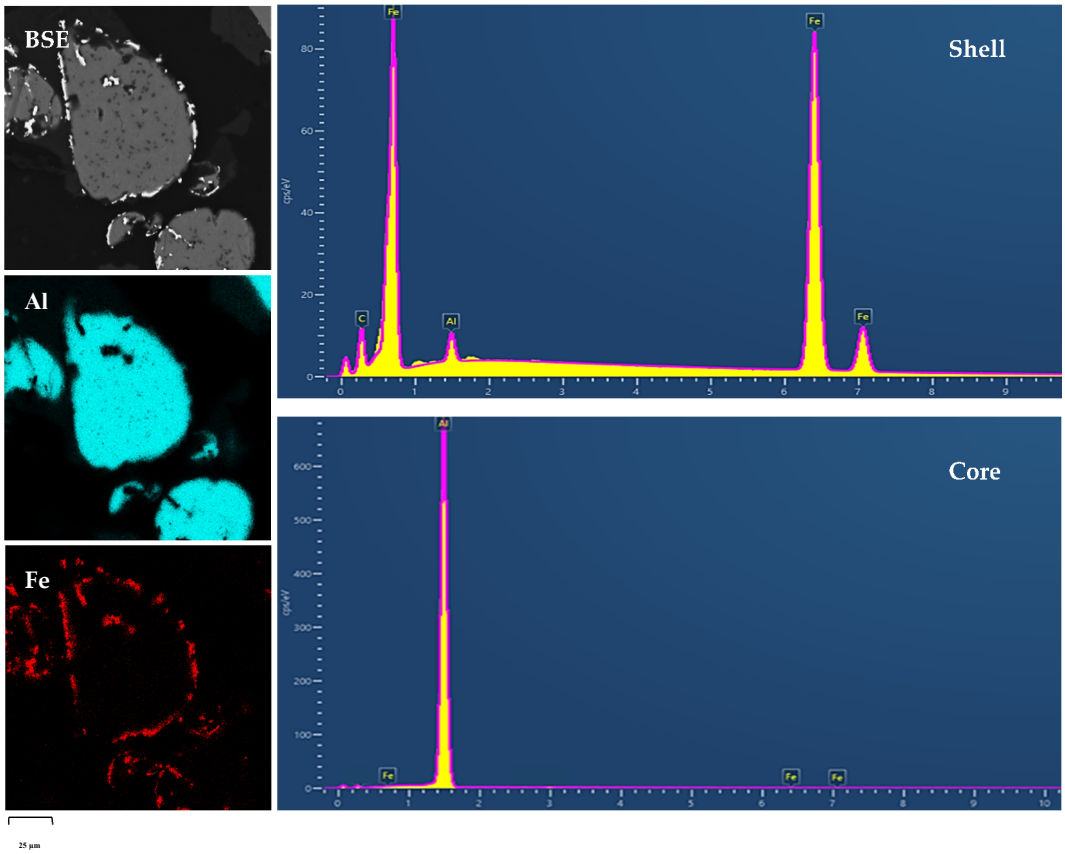

Figure 3. SEM image and EDS spectra of Fe-Al bimetallic material with a core-shell structure.

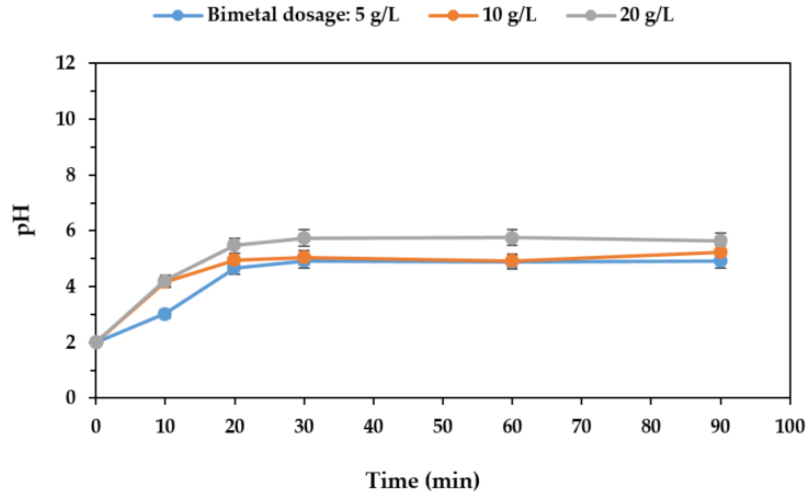

Figure 4. Variation in the pH of the combined AMD solution treated by the Fe-Al bimetal at a different time and bimetal dosage.

3.3. Metal Removal by the Fe-Al Bimetallic Material

The percent removal of various metals from the synthetic combined AMD treated by the Fe-Al bimetallic material for 90 min was compared and illustrated in Figure 5. What stands out in this figure is the higher uptake of Hg, As, Cu and Pb at all bimetal levels compared with Zn, Ni, and Mn. Experiments with 20 g/L of the bimetal resulted in significant removal of Hg (99.74%), As (99.80%), Cu (98.20%), and Pb (95.50%), while it dropped to 69.50% removal for Zn, 22.34% for Ni, and <5% for Mn. As previously stated, the higher standard redox potential of the aqueous contaminants than the Al and Fe is the underlying cause of a greater removal rate. Table 2 displays the standard reduction potential of various aqueous species in the experiments at 25 °C. The data are arranged in the increasing order of E^0, which means an increase in the tendency of species to get reduced. Therefore, under competitive conditions in the process, the loss of Hg, As, Cu, and Pb was higher than Ni, Zn, and Mn, as they have a greater attraction for electrons released from the bimetal.

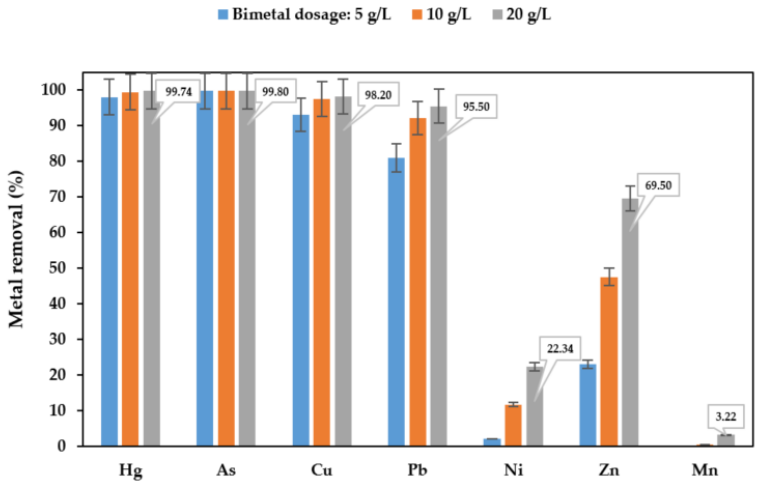

Figure 5. A comparison of the removal of various PTE from the synthetic combined AMD by Fe-Al bimetallic particles after 90 min and initial pH 2.

Table 2. Standard reduction potential of different species in aqueous solution at 25 °C [24,42].

Aqueous Species	Reduction Half Reactions	E^0 (V)
Aluminum (Al)	$Al^{3+} + 3e^- \rightarrow Al_{(S)}$	−1.68
Manganese (Mn)	$Mn^{2+} + 2e^- \rightarrow Mn_{(S)}$	−1.18
Zinc (Zn)	$Zn^{2+} + 2e^- \rightarrow Zn_{(S)}$	−0.76
Iron (Fe(II))	$Fe^{2+} + 2e^- \rightarrow Fe_{(S)}$	−0.44
Nickel (Ni)	$Ni^{2+} + 2e^- \rightarrow Ni_{(S)}$	−0.28
Lead (Pb)	$Pb^{2+} + 2e^- \rightarrow Pb_{(S)}$	−0.13
Copper (Cu(I))	$Cu^{2+} + e^- \rightarrow Cu^+$	+0.15
Arsenic (As(III))	$H_3AsO_3 + 3H^+ + 3e^- \rightarrow As + 3H_2O$	+0.24
Copper (Cu(II))	$Cu^{2+} + 2e^- \rightarrow Cu_{(S)}$	+0.34
Arsenic (As(V))	$H_3AsO_4 + 2H^+ + 2e^- \rightarrow HAsO_2 + 4H_2O$	+0.56
Iron (Fe(III))	$Fe^{3+} + e^- \rightarrow Fe^{2+}$	+0.77
Mercury (Hg)	$Hg^{2+} + 2e^- \rightarrow Hg_{(l)}$	+0.86

The variation of residual metal concentrations over time at different bimetal dosages (5, 10, and 20 g/L) and initial pH of 2 are shown in Figure 6. The initial Hg concentration in the solution (Figure 6a) dropped significantly in 10 min at all bimetal dosages, although the residual Hg(II) was slightly higher in the experiments with 5g/L bimetal (2.14 mg/L) compared to 10 and 20 g/L (<0.2 mg/L). In addition, ZVAl and ZVI on the bimetal surface, Fe^{2+} ions (E° (Fe^{3+}/Fe^{2+}) = +0.77) have also been considered as a reducing agent for Hg(II)

elimination from the solution [43]. Moreover, the increase in the solution pH to >4.5 in 20 min at various bimetal dosages, resulted in the precipitation of Fe (oxy)hydroxides on the bimetal surface (Figure 7a), which can sequester Hg(II) from the solution [43].

A similar trend to Hg was observed for the residual As and Cu concentrations (Figure 6b,c) within 90 min of AMD treatment using the bimetal. Despite that within 20 min of the process using 5 g/L bimetal As uptake was lower than that of 10, and 20 g/L, the removal rate was almost the same from 20 to 90 min. In addition, the initial Cu concentration of 53.44 mg/L went down to 3.5, 1.4, and 1 mg/L at 90 min for 5, 10, and 20 g/L bimetal, respectively. The higher bimetal concentrations performed more effectively for the Pb(II) reduction, so that the best result was obtained by using 20 g/L of the bimetal at 60 min (96% removal) (Figure 6d).

Prior studies [26,44] have reported the possible mechanisms for As removal by the Fe-Al bimetal as follows: (1) the adsorption of part of free As(III) by Fe-Al oxides on the bimetal surface at the initial stages of the process; (2) the oxidation of the majority of As(III) to As(V) by reactive oxygen species generated in the system, and the subsequent adsorption of As(V) by the Fe-Al (oxy)hydroxides on the bimetal surface; (3) the reduction of the adsorbed As(V) to As(III), and then to As(0) by Fe and Al (either directly or through the galvanic cell effect) in the anoxic inner layer of the bimetallic particles. Therefore, the observed discrepancy in the As uptake within 20 min of the process using different bimetal dosages corresponds most directly to the solution pH and the formation of the Fe-Al oxy-hydroxides on the bimetal (Figure 7a,b). For the AMD treated with 10 and 20 g/L bimetal, the pH values reached more than 4 in 10 min, while the same pH was recorded after 20 min for the experiment with 5 g/L bimetal (Figure 4). Considering that under acidic and circumneutral pH, the solubility, mobility, and toxicity of the As(III) is higher than As(V) species [45,46], the Fe-Al bimetal seems to be an effective material for the As remediation from the contaminated water.

According to the redox potential (Table 2), Cu(II) and Pb(II) can be easily reduced to Cu^0 and Pb^0 by both Fe and Al. Moreover, the reduction of Cu(II) to Cu(I) is also thermodynamically favored, resulting in the formation of insoluble Cu_2O [42]. However, Igarashi, et al. (2020) [47] have shown that Cu precipitation at pH < 6 is unfavorable and its reduction is mostly attributed to co-precipitation with Fe and Al oxy-hydroxides. The metal contaminants with more negative redox potential than Fe, including Ni, Zn, and Mn, are hard to be reduced by Fe. The reduction by ZVAl and adsorption may be the predominant removal mechanism as the bimetal surface became more negatively charged with increasing OH^- concentration, which enhanced the attraction between heavy metal ions and ZVI or ZVAl [28]. The higher removal of Zn, compared to Ni (Figure 6e,f), may be attributed to the adsorption by precipitated iron oxides on the bimetallic particles, which has been considered as a major Zn(II) removal mechanism by ZVI [48]. Moreover, due to the competitive effects, the uptake of Ni, Zn, and Mn by the bimetal may be hindered by Hg, As, Cu, and Pb ions. In addition, as can be seen in Figure 7c–e, the pH increase in the system was not sufficient to drive Mn, Zn, and Ni precipitation as they exist as aqueous species under the experimental conditions. As can be seen in Figure 6e–g, concentrations of Zn, Ni, and Mn decreased over the first 10 min of the reaction before increasing again from 10 to 30 min. The re-dissolution of these metal ions can be explained by the re-oxidation of deposited metals with the accumulated Fe(III) ((Fe^{3+}/Fe^{2+}) = +0.77). In addition, the concentration of heavy metal ions such as Zn, Ni, and Cu do not seem to be affected by the high concentration of Cl^- anion in the pH range of the experiments (pH of 2–4) as it causes an increase in the metal's solubility [49–51]. However, in the case of Hg, calomel (Hg_2Cl_2) precipitation may contribute to its reduction from the solution [52,53].

Regarding the presence of nitrate ions in the system, it should be noted that nitrate has a higher electron affinity than metal ions in the process meaning it is more likely to gain electrons released from the bimetal in the competitive system. In the Fe-Al bimetallic system, both Al and Fe are able to reduce nitrate ion to nitrite (NO_2^-) (E°= 0.965 V), then ammonia (NH_4^+) (E°= 0.897 V) or nitrogen gas [54,55]. Further research should be

undertaken to investigate the precise effect of NO_3^- and Cl^- ions on heavy metal removal from AMD and on the bimetal performance.

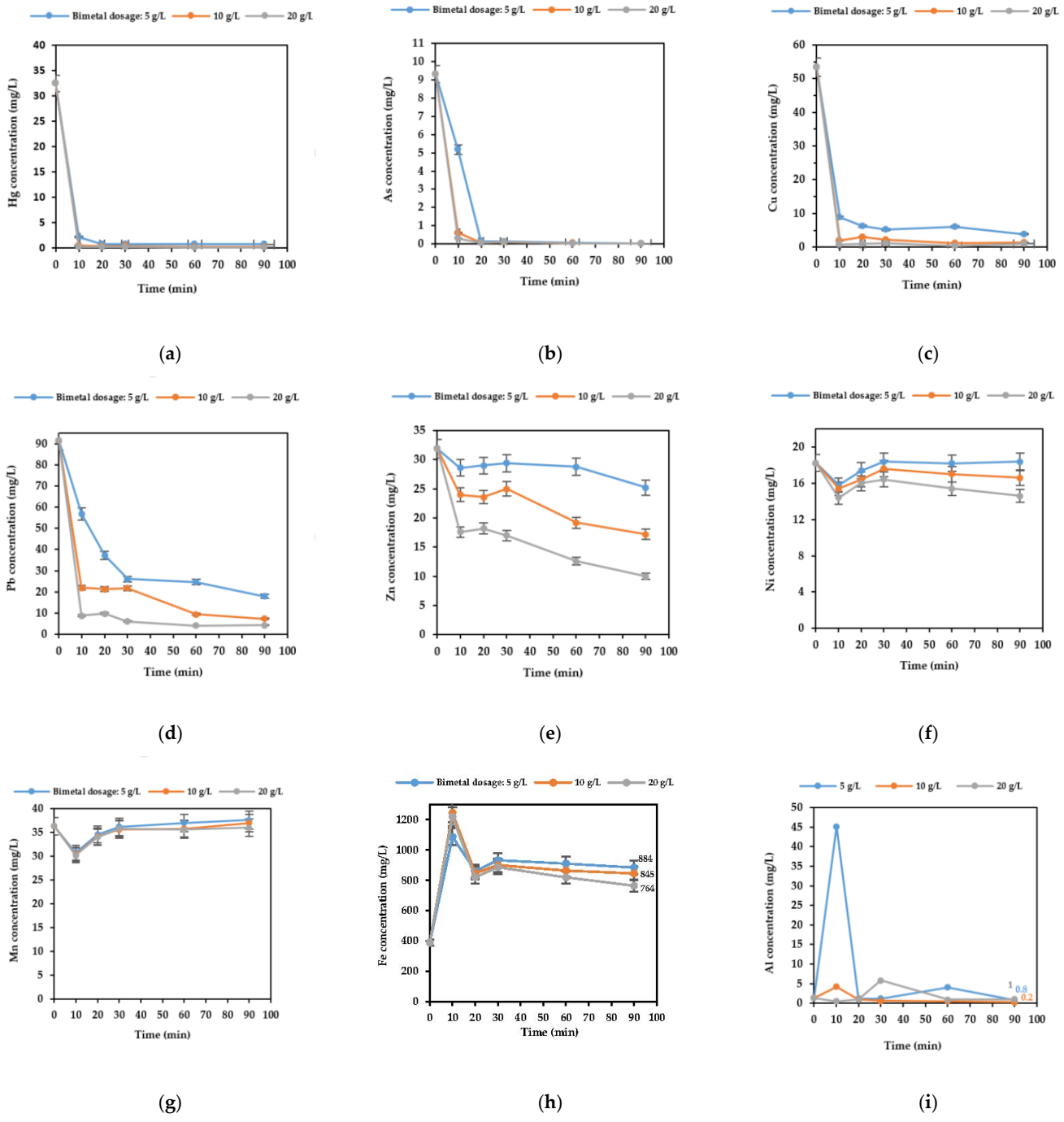

Figure 6. Variation of residual metal concentrations (**a**) As, (**b**) Hg, (**c**) Cu, (**d**) Pb, (**e**) Zn, (**f**) Ni, (**g**) Mn, (**h**) Fe, and (**i**) Al over time at different bimetal dosage (5, 10, and 20 g/L) and initial pH of 2.

The Fe corrosion (Equation (5)) led to a rise in its concentration in the solution within 10 min of the process (Figure 6h). However, it decreased after 10 min, which may be attributed to the precipitation of Fe ions by increasing the pH (Figure 7a). The total Fe ions concentration after 90 min of the process using 5, 10, and 20 g/L of the bimetal are 884, 845, and 764 mg/L, respectively. The pH rise driven by increasing the bimetal dosage can be the main reason for the lower dissolved Fe ions concentrations. As can be seen in Figure 7a (the dashed rectangle) in the experimental Eh range (0.5–0.21 V) and pH > 4,

Fe may precipitate as Schwertmannite or Magnetite. Moreover, depending on the Fe^{2+}, Fe^{3+}, and Cl^{-} concentrations, pH, and temperature of the reaction mixture, chloride ions may incorporate into the iron (oxy)hydroxide structure to form akaganetite [56,57], which has shown desirable sorption properties for PTE, such as As and Zn [58,59]. So, further research is needed to better understand the possibility of akaganetite formation under the experimental conditions of this study.

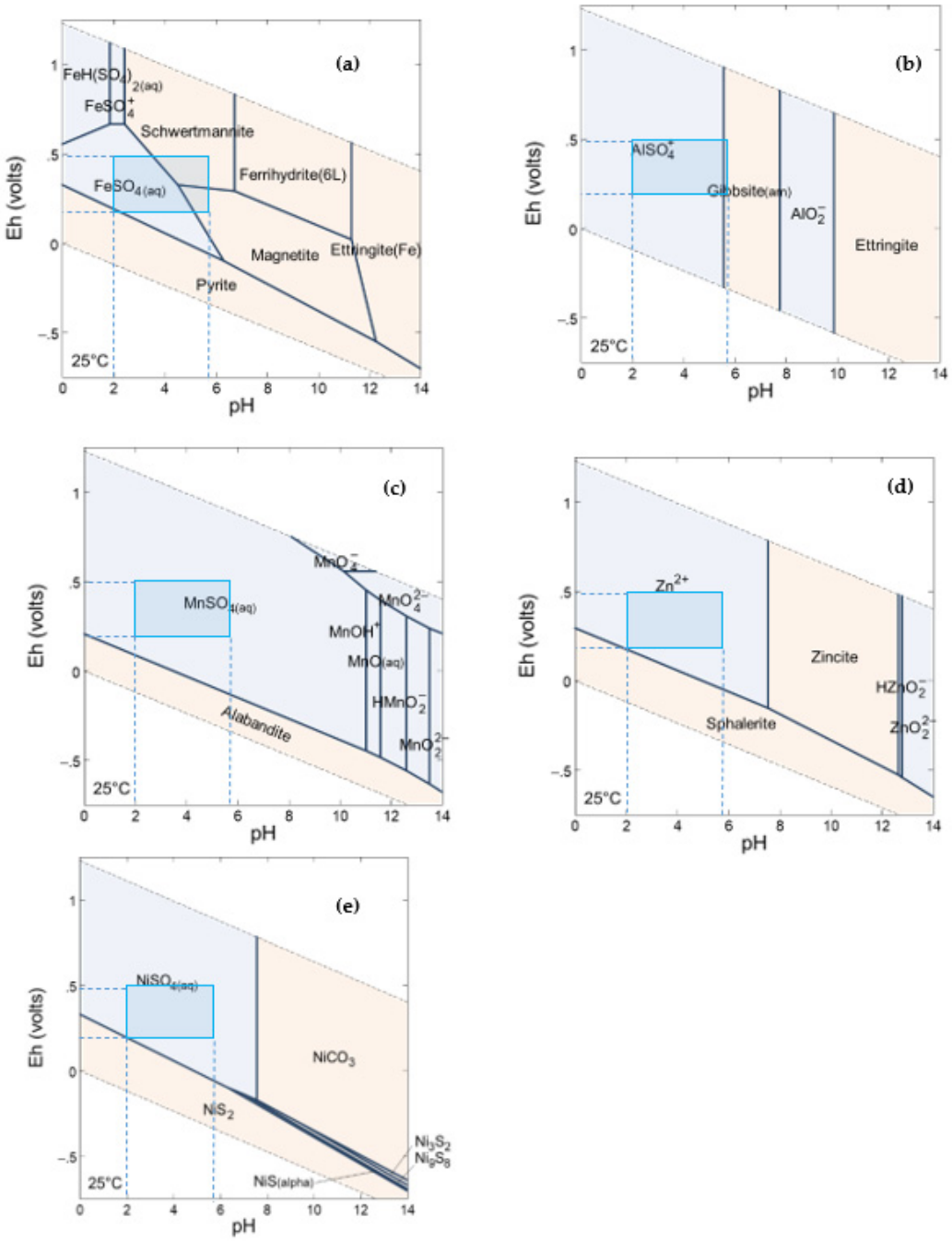

Figure 7. Eh-pH predominance diagram of (**a**) Fe^{3+} (activity = $10^{-2.65}$), (**b**) Al^{3+} (activity = $10^{-4.53}$), (**c**) Mn^{2+} (activity = $10^{-3.99}$), (**d**) Zn^{2+} (activity = $10^{-3.9}$), and (**e**) of Ni^{2+} (activity = $10^{-3.7}$) at 25 °C, 1.013 bars and activities of SO_4^{2-}, Na^{+} and Ca^{2+} equal to $10^{-1.6}$, $10^{-0.57}$ and $10^{-2.4}$, respectively. Carbonate was modelled in the system by equilibrating it with the average CO_2 in air (Fugacity = $10^{-3.5}$). The dashed rectangle refers to experimental conditions in this study.

Considering that the maximum recommended level of Fe in drinking water by the World Health Organization (WHO) is 2 mg/L [25], the release of Fe ions from the bimetal after the reaction with AMD is significant. However, Fe is less harmful compared to toxic heavy metals content in AMD and can be removed from the solution by a secondary neutralization process and converted to usable iron oxides as a raw material in pigments, ceramics, etc. [37]. The Al^{3+} concentrations in the final solutions are negligible, except for the experiment with 5 g/L of the bimetal within 10 min of the process in which the total dissolved AL^{3+} was 45 mg/L (Figure 6i). It is attributed to the solution pH, which is less than 3, and Al^{3+} is the predominant species (Figure 7b). In addition, the Al^{3+} concentration in the experiment using 10 g/L of the bimetal and the reaction time of 90 min meet the established limit in drinking water by WHO (0.2 mg/L) [25].

4. Conclusions

In this investigation, the synthesized Fe-Al bimetallic material has demonstrated high efficiency for a rapid removal of potentially toxic elements from the combined AMD-waste solutions resulting from refractory gold production. Owing to a greater tendency for electrons released from the bimetal, higher removal rate was obtained for Hg, As, Cu, and Pb than the Ni, Zn, and Mn. Experiments with 20 g/L of the bimetal resulted in significant removal of Hg (99.74%), As (99.80%), Cu (98.20%), and Pb (95.50%) in 90 min, while it dropped to 69.50% removal for Zn, 22.34% for Ni, and <5% for Mn. Therefore, the electrochemical reduction of PTE by the bimetal seems to be the major contributing mechanism. The findings of this study also indicate that the higher bimetal dosages result in the greater heavy metal uptake from the solution. Moreover, the corrosion of Fe and Al in the bimetallic system and consequently the release of Fe(III), Al(III), and OH^- ions into the solution led to the formation of Fe-Al (oxy)hydroxides which could sequester PTE, such as Hg and Zn, via adsorption. In addition, with respect to electrode potential of metal species, Fe(III) ions engaged in the re-oxidation of deposited Zn, and more significantly Mn and Ni, led to an increase in their concentrations after 10 min. The increase in the initial pH of 2 to more than 5 in 90 min using Fe-Al bimetallic particles is promising in AMD remediation as it can reduce the amount of alkaline reagents. Nearly no Al ions were detected in the solutions at higher bimetal concentrations. Although the Fe release from the bimetal was high, it can be precipitated and converted to a valuable by-product such as iron pigments. However, more research on this topic needs to be undertaken to identify the influencing parameters, characterize and analyze the surface chemistry of bimetallic particles after reaction with PTE and measure the elemental composition, and chemical and electronic state of the elements on the bimetal. Chloride ions in the studied system may affect the process by akaganeite formation and changing the stability of PTE. Moreover, the higher electrode potential of nitrate compared to Fe, Al, and other metals in the process, could mean it has a higher tendency to gain electrons and get reduced. However, further studies regarding the precise effect of Cl^- and NO_3^- on PTE removal and bimetal performance is strongly recommended. The reversibility of the process and reusability of the bimetal also warrant additional investigation.

Author Contributions: Conceptualization, R.D.A., C.B.T., E.A.; methodology, E.A. and R.D.A.; validation and analysis, E.A., Z.W., R.D.A. and Z.Q.; writing—original draft preparation, E.A. and Z.W.; writing—review and editing, R.D.A., B.T., C.B.T. and E.A.; supervision, R.D.A. and B.T.; All authors have read and agreed to the published version of the manuscript.

Funding: This research received no external funding.

Data Availability Statement: Data sharing is not applicable to this article.

Acknowledgments: Curtin University's Strategic Scholarship is gratefully acknowledged for the PhD scholarship granted to Elham Aghaei.

Conflicts of Interest: The authors declare no conflict of interest.

References

1. Park, I.; Tabelin, C.B.; Jeon, S.; Li, X.; Seno, K.; Ito, M.; Hiroyoshi, N. A review of recent strategies for acid mine drainage prevention and mine tailings recycling. *Chemosphere* **2019**, *219*, 588–606. [CrossRef] [PubMed]
2. Moodley, I.; Sheridan, C.M.; Kappelmeyer, U.; Akcil, A. Environmentally sustainable acid mine drainage remediation: Research developments with a focus on waste/by-products. *Miner. Eng.* **2018**, *126*, 207–220. [CrossRef]
3. Wilkin, R.T.; McNeil, M.S. Laboratory evaluation of zero-valent iron to treat water impacted by acid mine drainage. *Chemosphere* **2003**, *53*, 715–725. [CrossRef]
4. Wills, B.A.; Finch, J.A. Chapter 16—Tailings Disposal. In *Wills' Mineral Processing Technology (Eighth Edition)*; Wills, B.A., Finch, J.A., Eds.; Butterworth-Heinemann: Boston, FL, USA, 2016; pp. 439–448. [CrossRef]
5. Kefeni, K.K.; Msagati, T.A.M.; Mamba, B.B. Acid mine drainage: Prevention, treatment options, and resource recovery: A review. *J. Clean. Prod.* **2017**, *151*, 475–493. [CrossRef]
6. Naidu, G.; Ryu, S.; Thiruvenkatachari, R.; Choi, Y.; Jeong, S.; Vigneswaran, S. A critical review on remediation, reuse, and resource recovery from acid mine drainage. *Environ. Pollut.* **2019**, *247*, 1110–1124. [CrossRef] [PubMed]
7. Dold, B. Evolution of Acid Mine Drainage Formation in Sulphidic Mine Tailings. *Minerals* **2014**, *4*, 621–641. [CrossRef]
8. Diao, Z.; Shi, T.; Wang, S.; Huang, X.; Zhang, T.; Tang, Y.; Zhang, X.; Qiu, R. Silane-based coatings on the pyrite for remediation of acid mine drainage. *Water Res.* **2013**, *47*, 4391–4402. [CrossRef] [PubMed]
9. Shu, X.; Dang, Z.; Zhang, Q.; Yi, X.; Lu, G.; Guo, C.; Yang, C. Passivation of metal-sulfide tailings by covalent coating. *Miner. Eng.* **2013**, *42*, 36–42. [CrossRef]
10. Alakangas, L.; Andersson, E.; Mueller, S. Neutralization/prevention of acid rock drainage using mixtures of alkaline by-products and sulfidic mine wastes. *Environ. Sci. Pollut. Res.* **2013**, *20*, 7907–7916. [CrossRef]
11. Nason, P.; Johnson, R.H.; Neuschütz, C.; Alakangas, L.; Öhlander, B. Alternative waste residue materials for passive in situ prevention of sulfide-mine tailings oxidation: A field evaluation. *J. Hazard. Mater.* **2014**, *267*, 245–254. [CrossRef]
12. Jin, S.; Fallgren, P.H.; Morris, J.M.; Cooper, J.S. Source Treatment of Acid Mine Drainage at a Backfilled Coal Mine Using Remote Sensing and Biogeochemistry. *Water Air Soil Pollut.* **2008**, *188*, 205–212. [CrossRef]
13. Li, X.; Hiroyoshi, N.; Tabelin, C.B.; Naruwa, K.; Harada, C.; Ito, M. Suppressive effects of ferric-catecholate complexes on pyrite oxidation. *Chemosphere* **2019**, *214*, 70–78. [CrossRef]
14. Jones, S.N.; Cetin, B. Evaluation of waste materials for acid mine drainage remediation. *Fuel* **2017**, *188*, 294–309. [CrossRef]
15. Bortnikova, S.; Gaskova, O.; Yurkevich, N.; Saeva, O.; Abrosimova, N. Chemical Treatment of Highly Toxic Acid Mine Drainage at A Gold Mining Site in Southwestern Siberia, Russia. *Minerals* **2020**, *10*, 867. [CrossRef]
16. Pat-Espadas, A.M.; Loredo Portales, R.; Amabilis-Sosa, L.E.; Gómez, G.; Vidal, G. Review of Constructed Wetlands for Acid Mine Drainage Treatment. *Water* **2018**, *10*, 1685. [CrossRef]
17. Fytas, K. Use of permeable reactive barriers to treat acid mine effluents. *Int. J. Min. Reclam. Environ.* **2010**, *24*, 206–215. [CrossRef]
18. Gibert, O.; Rötting, T.; Cortina, J.L.; de Pablo, J.; Ayora, C.; Carrera, J.; Bolzicco, J. In-situ remediation of acid mine drainage using a permeable reactive barrier in Aznalcóllar (Sw Spain). *J. Hazard. Mater.* **2011**, *191*, 287–295. [CrossRef] [PubMed]
19. Kaksonen, A.H.; Puhakka, J.A. Sulfate Reduction Based Bioprocesses for the Treatment of Acid Mine Drainage and the Recovery of Metals. *Eng. Life Sci.* **2007**, *7*, 541–564. [CrossRef]
20. Gitari, M.W.; Petrik, L.F.; Etchebers, O.; Key, D.L.; Iwuoha, E.; Okujeni, C. Treatment of acid mine drainage with fly ash: Removal of major contaminants and trace elements. *J. Environ. Sci. Health Part A Toxic/Hazard. Subst. Environ. Eng.* **2006**, *41*, 1729–1747. [CrossRef]
21. Wu, Y.; Guan, C.-Y.; Griswold, N.; Hou, L.-Y.; Fang, X.; Hu, A.; Hu, Z.-Q.; Yu, C.-P. Zero-valent iron-based technologies for removal of heavy metal(loid)s and organic pollutants from the aquatic environment: Recent advances and perspectives. *J. Clean. Prod.* **2020**, *277*, 123478. [CrossRef]
22. Obiri-Nyarko, F.; Grajales-Mesa, S.J.; Malina, G. An overview of permeable reactive barriers for in situ sustainable groundwater remediation. *Chemosphere* **2014**, *111*, 243–259. [CrossRef] [PubMed]
23. Nidheesh, P.V.; Khatri, J.; Anantha Singh, T.S.; Gandhimathi, R.; Ramesh, S.T. Review of zero-valent aluminium based water and wastewater treatment methods. *Chemosphere* **2018**, *200*, 621–631. [CrossRef] [PubMed]
24. Chen, L.-H.; Huang, C.-C.; Lien, H.-L. Bimetallic iron–aluminum particles for dechlorination of carbon tetrachloride. *Chemosphere* **2008**, *73*, 692–697. [CrossRef] [PubMed]
25. Fu, F.; Cheng, Z.; Dionysiou, D.D.; Tang, B. Fe/Al bimetallic particles for the fast and highly efficient removal of Cr(VI) over a wide pH range: Performance and mechanism. *J. Hazard. Mater.* **2015**, *298*, 261–269. [CrossRef]
26. Cheng, Z.; Fu, F.; Dionysiou, D.D.; Tang, B. Adsorption, oxidation, and reduction behavior of arsenic in the removal of aqueous As(III) by mesoporous Fe/Al bimetallic particles. *Water Res.* **2016**, *96*, 22–31. [CrossRef]
27. Xiang, S.; Cheng, W.; Nie, X.; Ding, C.; Yi, F.; Asiri, A.M.; Marwani, H.M. Zero-valent iron-aluminum for the fast and effective U(VI) removal. *J. Taiwan Inst. Chem. Eng.* **2018**, *85*, 186–192. [CrossRef]
28. Han, W.; Fu, F.; Cheng, Z.; Tang, B.; Wu, S. Studies on the optimum conditions using acid-washed zero-valent iron/aluminum mixtures in permeable reactive barriers for the removal of different heavy metal ions from wastewater. *J. Hazard. Mater.* **2016**, *302*, 437–446. [CrossRef]
29. Iakovleva, E.; Mäkilä, E.; Salonen, J.; Sitarz, M.; Wang, S.; Sillanpää, M. Acid mine drainage (AMD) treatment: Neutralization and toxic elements removal with unmodified and modified limestone. *Ecol. Eng.* **2015**, *81*, 30–40. [CrossRef]

30. Marsden, J.O.; House, C.I. *Chemistry of Gold Extraction*, 2nd ed.; SME: Littleton, CO, USA, 2009.
31. Deschenes, G.; Lastra, R.; Brown, J.R.; Jin, S.; May, O.; Ghali, E. Effect of lead nitrate on cyanidation of gold ores: Progress on the study of the mechanisms. *Miner. Eng.* **2000**, *13*, 1263–1279. [CrossRef]
32. Deschênes, G.; McMullen, J.; Ellis, S.; Fulton, M.; Atkin, A. Investigation on the cyanide leaching optimization for the treatment of KCGM gold flotation concentrate—phase 1. *Miner. Eng.* **2005**, *18*, 832–838. [CrossRef]
33. Ali, R.; Turner, J. A Study of the Suitability of Saline Surface Water for Recharging the Hypersaline Palaeochannel Aquifers of the Eastern Goldfields of Western Australia. *Mine Water Environ.* **2004**, *23*, 110–118. [CrossRef]
34. Muir, D.M. *Gold Processing with Saline Water*; The Australasian Institute of Mining and Metallurgy: Carlton, Australia, 1994.
35. Bethke, C.M.; Yeakel, S. *The Geochemist's Workbench—A User's Guide to GSS, Rxn, Act2, Tact, Spec8, React, Gtplot, X1t, X2t, and Xtplot*; Aqueous Solutions LLC: Urbana, IL, USA, 2011.
36. Blanc, P.; Lassin, A.; Piantone, P.; Azaroual, M.; Jacquemet, N.; Fabbri, A.; Gaucher, E.C. Thermoddem: A geochemical database focused on low temperature water/rock interactions and waste materials. *Appl. Geochem.* **2012**, *27*, 2107–2116. [CrossRef]
37. Simate, G.S.; Ndlovu, S. Acid mine drainage: Challenges and opportunities. *J. Environ. Chem. Eng.* **2014**, *2*, 1785–1803. [CrossRef]
38. Lien, H.-L.; Yu, C.-H.; Kamali, S.; Sahu, R.S. Bimetallic Fe/Al system: An all-in-one solid-phase Fenton reagent for generation of hydroxyl radicals under oxic conditions. *Sci. Total Environ.* **2019**, *673*, 480–488. [CrossRef] [PubMed]
39. Wu, S.; Yang, S.; Liu, S.; Zhang, Y.; Ren, T.; Zhang, Y. Enhanced reactivity of zero-valent aluminum with ball milling for phenol oxidative degradation. *J. Colloid Interface Sci.* **2020**, *560*, 260–272. [CrossRef]
40. Bokare, A.D.; Choi, W. Zero-valent aluminum for oxidative degradation of aqueous organic pollutants. *Environ. Sci. Technol.* **2009**, *43*, 7130–7135. [CrossRef]
41. Yang, S.; Zheng, D.; Ren, T.; Zhang, Y.; Xin, J. Zero-valent aluminum for reductive removal of aqueous pollutants over a wide pH range: Performance and mechanism especially at near-neutral pH. *Water Res.* **2017**, *123*, 704–714. [CrossRef] [PubMed]
42. O'Carroll, D.; Sleep, B.; Krol, M.; Boparai, H.; Kocur, C. Nanoscale zero valent iron and bimetallic particles for contaminated site remediation. *Adv. Water Resour.* **2013**, *51*, 104–122. [CrossRef]
43. Vernon, J.D.; Bonzongo, J.-C.J. Volatilization and sorption of dissolved mercury by metallic iron of different particle sizes: Implications for treatment of mercury contaminated water effluents. *J. Hazard. Mater.* **2014**, *276*, 408–414. [CrossRef] [PubMed]
44. Meng, C.; Mao, Q.; Luo, L.; Zhang, J.; Wei, J.; Yang, Y.; Tan, M.; Peng, Q.; Tang, L.; Zhou, Y. Performance and mechanism of As(III) removal from water using Fe-Al bimetallic material. *Sep. Purif. Technol.* **2018**, *191*, 314–321. [CrossRef]
45. Liu, F.; Yang, W.; Li, W.; Zhao, G.-C. Simultaneous Oxidation and Sequestration of Arsenic(III) from Aqueous Solution by Copper Aluminate with Peroxymonosulfate: A Fast and Efficient Heterogeneous Process. *ACS Omega* **2021**, *6*, 1477–1487. [CrossRef] [PubMed]
46. Tabelin, C.B.; Igarashi, T.; Villacorte-Tabelin, M.; Park, I.; Opiso, E.M.; Ito, M.; Hiroyoshi, N. Arsenic, selenium, boron, lead, cadmium, copper, and zinc in naturally contaminated rocks: A review of their sources, modes of enrichment, mechanisms of release, and mitigation strategies. *Sci. Total Environ.* **2018**, *645*, 1522–1553. [CrossRef]
47. Igarashi, T.; Herrera, P.S.; Uchiyama, H.; Miyamae, H.; Iyatomi, N.; Hashimoto, K.; Tabelin, C.B. The two-step neutralization ferrite-formation process for sustainable acid mine drainage treatment: Removal of copper, zinc and arsenic, and the influence of coexisting ions on ferritization. *Sci. Total Environ.* **2020**, *715*, 136877. [CrossRef]
48. Rangsivek, R.; Jekel, M.R. Removal of dissolved metals by zero-valent iron (ZVI): Kinetics, equilibria, processes and implications for stormwater runoff treatment. *Water Res.* **2005**, *39*, 4153–4163. [CrossRef]
49. Beverskog, B.; Puigdomenech, I. *Pourbaix Diagrams for the System Copper-Chlorine at 5–100 °C*; Swedish Nuclear Power Inspectorate: Stockholm, Sweden, 1998; p. 56.
50. He, D.; Zeng, L.; Zhang, G.; Guan, W.; Cao, Z.; Li, Q.; Wu, S. Extraction behavior and mechanism of nickel in chloride solution using a cleaner extractant. *J. Clean. Prod.* **2020**, *242*, 118517. [CrossRef]
51. Stec, M.; Jagustyn, B.; Słowik, K.; Ściążko, M.; Iluk, T. Influence of High Chloride Concentration on pH Control in Hydroxide Precipitation of Heavy Metals. *J. Sustain. Metall.* **2020**, *6*, 239–249. [CrossRef]
52. Grassi, S.; Netti, R. Sea water intrusion and mercury pollution of some coastal aquifers in the province of Grosseto (Southern Tuscany—Italy). *J. Hydrol.* **2000**, *237*, 198–211. [CrossRef]
53. Spyropoulou, A.; Lazarou, Y.G.; Laspidou, C. Mercury Speciation in the Water Distribution System of Skiathos Island, Greece. *Proceedings* **2018**, *2*, 668. [CrossRef]
54. Liu, Y.; Wang, J. Reduction of nitrate by zero valent iron (ZVI)-based materials: A review. *Sci. Total Environ.* **2019**, *671*, 388–403. [CrossRef]
55. Esfahani, A.R.; Datta, T. Nitrate removal from water using zero-valent aluminium. *Water Environ. J.* **2020**, *34*, 25–36. [CrossRef]
56. Scheck, J.; Lemke, T.; Gebauer, D. The Role of Chloride Ions during the Formation of Akaganéite Revisited. *Minerals* **2015**, *5*, 778–787. [CrossRef]
57. Rémazeilles, C.; Refait, P. On the formation of β-FeOOH (akaganéite) in chloride-containing environments. *Corros. Sci.* **2007**, *49*, 844–857. [CrossRef]
58. Zhao, J.; Lin, W.; Chang, Q.; Li, W.; Lai, Y. Adsorptive characteristics of akaganeite and its environmental applications: A review. *Environ. Technol. Rev.* **2012**, *1*, 114–126. [CrossRef]
59. Deliyanni, E.A.; Bakoyannakis, D.N.; Zouboulis, A.I.; Peleka, E. Removal of Arsenic and Cadmium by Akaganeite Fixed-Beds. *Sep. Sci. Technol.* **2003**, *38*, 3967–3981. [CrossRef]